Available online at www.sciencedirect.com
SCIENCE DIRECT®
Journal of Computational Physics 191 (2003) 525–541
JOURNAL OF COMPUTATIONAL PHYSICS
www.elsevier.com/locate/jcp

Long-time numerical computation of electromagnetic fields in the vicinity of a relativistic source

Igor Zagorodnov *,[1], Rolf Schuhmann, Thomas Weiland

Technische Universität Darmstadt, FB 18, Computational Electromagnetics Laboratory (TEMF), Schloßgartenstraße 8, D-64289 Darmstadt, Germany

Received 20 March 2003; received in revised form 11 June 2003; accepted 22 June 2003

Abstract

We propose an implicit scheme for the calculation of electromagnetic fields in the vicinity of short electron bunches moving in a transversally bounded domain, as it has place in particle accelerators. The scheme is able to accurately model curved boundaries and does not suffer from dispersion in direction of motion. It is based on splitting the discrete curl operator in its transversal and longitudinal parts. Unlike previous conformal schemes the new method has a second order convergence without the need to reduce the maximal stable time step of the conventional staircase approach. This feature allows the usage of a moving mesh easily. Several numerical examples are presented and the algorithm is compared to other approaches.

Keywords: Maxwell's equations; FDTD; Finite integration; Conformal; Wake field

1. Introduction

Recent accelerator applications require beams of high intensities. As the beam intensity is increased, the electromagnetic fields self-generated by the beam, particularly the fields generated by the beam interacting with its surroundings (wake fields), can become sufficiently strong and lead to an instability and subsequent beam loss [1]. The subject of collective instabilities in high energy accelerators has been studied since the late 1950s. In many cases finite difference methods can be applied successfully for calculation of wake fields in accelerators [2,3]. However the existing computer codes experience severe problems in short range wake field calculation for ultra short bunches [4]. Two main sources of such problems are the numerical grid dispersion and the staircase geometry approximation of standard Cartesian or cylindrical computational grids.

As an effective cure of the dispersion problem a numerical scheme without dispersion in longitudinal direction can be used as it is shown in [4,12] for the scalar wave equation. In order to develop a scheme

* Corresponding author. Tel.: +49-61561-164-787; fax: +49-6151-164-611.
E-mail addresses: zagorodnov@temf.de, zagor@temf.tu-darmstadt.de (I. Zagorodnov), schuhmann@temf.de (R. Schuhmann), weiland@temf.de (T. Weiland).
[1] Work supported in part by the Deutsche Forschungsgemeinschaft, project 1239/22-1.

0021-9991/$ - see front matter © 2003 Elsevier B.V. All rights reserved.
doi:10.1016/S0021-9991(03)00329-2

without dispersion in longitudinal direction for the vectorial problem we split the curl operator in the transversal and the longitudinal parts and use an implicit scheme based on the transversal part. The new scheme is conditionally stable and allows using the "magic" time step equal to the space step in the longitudinal direction over velocity of light.

To overcome the staircase problem a conformal scheme described in paper [5] is adopted. Unlike other conformal approaches this scheme is second order convergent without the need to reduce the maximal stable time step of the conventional staircase method. This feature allows to use a moving mesh and the "magic" time step without a need for interpolation. With this choice the scheme allows for a non-deteriorating calculation of the solution for as long as necessary.

In Section 2 we state the problem. In the third and fourth part the implicit scheme is introduced. In the fifth part the realization of the scheme for the rotationally symmetric case and a staircase approximation is described, and then in the next section the conformal second order convergent scheme is developed. In the seventh part a new algorithm for the indirect integration of the wake potential is introduced. Finally we show several numerical examples and compare the scheme with other approaches.

2. Formulation of the problem

We consider a mixed Cauchy problem: for a bunch moving with the velocity of light c and characterized by a charge distribution ρ find the electromagnetic fields $\vec{E},\vec{H}$ in a domain Ω which is bounded transversally by a perfect conductor $\partial\Omega$. The bunch introduces an electric current $\vec{j}=\vec{c}\rho$ and thus we have to solve for

$$\begin{aligned}
&\nabla\times\vec{H}=\frac{\partial}{\partial t}\vec{D}+\vec{j},\quad \nabla\times\vec{E}=-\frac{\partial}{\partial t}\vec{B},\\
&\nabla\cdot\vec{D}=\rho,\quad \nabla\cdot\vec{B}=0,\\
&\vec{H}=\mu^{-1}\vec{B},\quad \vec{D}=\varepsilon\vec{E},\\
&\vec{E}(t=0)=\vec{E}_0,\quad \vec{H}(t=0)=\vec{H}_0,\ \ x\in\Omega,\\
&\vec{n}\times\vec{E}=0,\quad x\in\partial\Omega.
\end{aligned}\tag{1}$$

The full electromagnetic fields $\vec{D},\vec{H}$ can be decomposed into the fields of the bunch in free space $\vec{D}^0,\vec{H}^0$ and a scattered field

$$\vec{D}^{\mathrm{sc}}=\vec{D}-\vec{D}^0,\quad \vec{H}^{\mathrm{sc}}=\vec{H}-\vec{H}^0.\tag{2}$$

The scattered field even in inhomogeneous regions can be presented by a vector potential $\vec{A}$:

$$\vec{D}^{\mathrm{sc}}=\nabla\times\vec{A},\quad \vec{H}^{\mathrm{sc}}=\frac{\partial}{\partial t}\vec{A}.\tag{3}$$

Substitution of the presentation (3) in the system (1) defines the problem formulation for the vector potential $\vec{A}$:

$$\begin{aligned}
&\nabla\times\varepsilon^{-1}\nabla\times\vec{A}=-\frac{\partial^2}{\partial t^2}\mu\vec{A}-\vec{j}^{\mathrm{sc}},\quad \vec{j}^{\mathrm{sc}}=\nabla\times\varepsilon^{-1}\vec{D}^0+\frac{\partial}{\partial t}\mu\vec{H}^0,\\
&\nabla\cdot\mu\left(\frac{\partial}{\partial t}\vec{A}+\vec{H}^0\right)=0,\quad \vec{A}(t=0)=\vec{A}_0,\ \ x\in\Omega,\\
&\vec{n}\cdot\vec{A}=-\int_{-\infty}^{t}\vec{n}\cdot\vec{H}^0\,\mathrm{d}\tau,\quad \vec{n}\times\nabla\times\vec{A}=-\int_{-\infty}^{t}\vec{n}\times\nabla\times\vec{H}^0\,\mathrm{d}\tau,\ \ x\in\partial\Omega,
\end{aligned}\tag{4}$$

where $\vec{A}_0$ is an initial value of the vector potential which has to be consistent with the initial fields $\vec{E}_0, \vec{H}_0$ of (1). In accelerator applications the studied structure usually is supplied by ingoing and outgoing pipes, and the analytical solution in the pipe can be used as initial condition.

In the following only vacuum regions Ω will be considered, i.e., the term $\vec{j}^{\text{sc}}$ is equal to zero and the excitation is imbedded in the boundary conditions (as is typical for scattered field formulations).

3. The finite integration technique

The new scheme will be introduced in context of the finite integration technique (FIT, [6,7]).

We consider Maxwell's Eq. (1) in their integral form on a domain $\Omega \subset R^3$, with linear non-dispersive constitutive relations:

$$\begin{aligned}
&\oint_{\partial S} \vec{E} \cdot \mathrm{d}\vec{l} = -\frac{\mathrm{d}}{\mathrm{d}t} \int_S \vec{B} \cdot \mathrm{d}\vec{s}, \quad \oint_{\partial S} \vec{H} \cdot \mathrm{d}\vec{l} = \frac{\mathrm{d}}{\mathrm{d}t} \int_S \vec{D} \cdot \mathrm{d}\vec{s} + \int_S \vec{J} \cdot \mathrm{d}\vec{s}, \ \forall S \subset \Omega, \\
&\oint_{\partial V} \vec{D} \cdot \mathrm{d}\vec{s} = \int_V \rho \, \mathrm{d}v, \quad \oint_{\partial V} \vec{B} \cdot \mathrm{d}\vec{s} = 0, \ \forall V \subset \Omega, \\
&\vec{D} = \varepsilon \vec{E}, \quad \vec{B} = \mu \vec{H}, \ \forall x \in \Omega.
\end{aligned} \tag{5}$$

Let us start by introducing a grid-based decomposition of the entire computation domain into two dual cell complexes K and $\tilde{K}$. We use here a three-dimensional cylindrical mesh in z, r, φ coordinates with corresponding numeration of the mesh by i, j, k indexes. Unlike in finite difference methods we do not start by allocating field components but rather by allocating the electric voltage along mesh edges and the magnetic flux through mesh cell facets as computational unknowns or state variables, respectively:

$$\begin{aligned}
&\widehat{e}_\vartheta = \int_{L_\vartheta} \vec{E} \cdot \mathrm{d}\vec{l}, \quad \widehat{h}_\vartheta = \int_{\tilde{L}_\vartheta} \vec{H} \cdot \mathrm{d}\vec{l}, \\
&\widehat{\widehat{d}}_\vartheta = \int_{\tilde{S}_\vartheta} \vec{D} \cdot \mathrm{d}\vec{s}, \quad \widehat{\widehat{b}}_\vartheta = \int_{S_\vartheta} \vec{B} \cdot \mathrm{d}\vec{s}, \quad \widehat{\widehat{j}}_\vartheta = \int_{\tilde{S}_\vartheta} \vec{J} \cdot \mathrm{d}\vec{s},
\end{aligned}$$

where ϑ is a mesh multi-index and $L_\vartheta, S_\vartheta \in K, \tilde{L}_\vartheta, \tilde{S}_\vartheta \in \tilde{K}$. Solving Faraday's Law in integral form for the front surface shown in Fig. 1 yields: $-\widehat{e}_{rijk} - \widehat{e}_{zij+1k} + \widehat{e}_{ri+1jk} + \widehat{e}_{zijk} = -(\mathrm{d}/\mathrm{d}t)\widehat{\widehat{b}}_{\varphi ijk}$. Note, that this

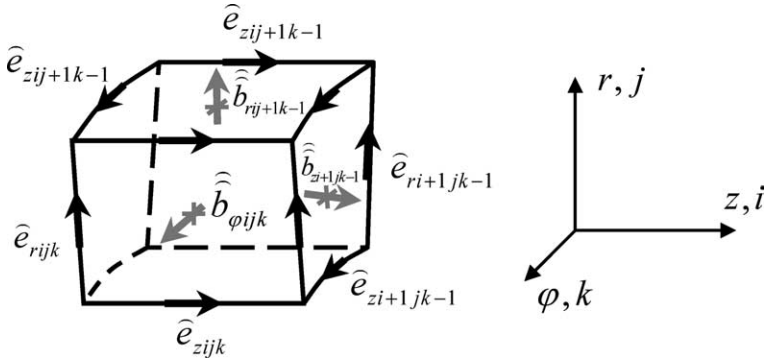

Fig. 1. Unit cell and state variables of the FIT.

representation is still exact, as $\widehat{e}_\vartheta$ is (by definition) the exact electric voltage along one edge of the surface, and similarly $\widehat{\widehat{b}}_\vartheta$ represents the exact value of the magnetic flux density integral over the cell surface.

If we compose column vectors $\widehat{\mathbf{e}}$ and $\widehat{\widehat{\mathbf{b}}}$ out of all voltage- and flux-components, we can write the combination of all equations over all surfaces in an elegant matrix form as

$$\mathbf{C}\widehat{\mathbf{e}} = -\frac{\mathrm{d}}{\mathrm{d}t}\widehat{\widehat{\mathbf{b}}}.$$

The matrix $\mathbf{C}$ picks the affected components out of the long vector to make up the corresponding equation. $\mathbf{C}$ is thus the discrete curl operator over the mesh K. On $\{u, v, w\}$-coordinate grids (like the cylindrical grid chosen here) with an appropriate indexing scheme the curl matrix has an 3×3 block structure:

$$\mathbf{C} = \begin{pmatrix} \mathbf{0} & -\mathbf{P}_w & \mathbf{P}_v \\ \mathbf{P}_w & \mathbf{0} & -\mathbf{P}_u \\ -\mathbf{P}_v & \mathbf{P}_u & \mathbf{0} \end{pmatrix}.$$

The two-banded, topological $\mathbf{P}_{\{u,v,w\}}$-matrices take the role of discrete partial differential-operators [8].

The second important differential operator in Maxwell's Eq. (5) is the div operator. In order to construct a discrete divergence operator we integrate Maxwell's equation $\oint_{\partial V} \vec{B} \cdot \mathrm{d}\vec{s} = 0$ over the entire surface of a mesh cell depicted in Fig. 1. From adding up the six relevant fluxes for each cell and by writing down all such equations for the entire cell complex we obtain a discrete analogue to the div-equation:

$$\mathbf{S}\widehat{\widehat{\mathbf{b}}} = \mathbf{0}, \quad \mathbf{S} = (\,\mathbf{P}_u \quad \mathbf{P}_v \quad \mathbf{P}_w\,).$$

After an equivalent procedure for the remaining Maxwell equations by means of a dual mesh $\tilde{K}$ we obtain a set of four discrete equations replacing Maxwell's equation on a grid doublet:

$$\begin{aligned} &\mathbf{C}\widehat{\mathbf{e}} = -\frac{\mathrm{d}}{\mathrm{d}t}\widehat{\widehat{\mathbf{b}}}, \quad \tilde{\mathbf{C}}\widehat{\mathbf{h}} = \frac{\mathrm{d}}{\mathrm{d}t}\widehat{\widehat{\mathbf{d}}} + \widehat{\widehat{\mathbf{j}}}, \\ &\mathbf{S}\widehat{\widehat{\mathbf{b}}} = \mathbf{0}, \quad \tilde{\mathbf{S}}\widehat{\widehat{\mathbf{d}}} = \mathbf{q}. \end{aligned} \tag{6}$$

They are completed by the discrete form of the material relations (constitutive equations) which appear (in the simplest linear case) as matrix equations

$$\widehat{\widehat{\mathbf{d}}} = \mathbf{M}_\varepsilon\widehat{\mathbf{e}}, \quad \widehat{\widehat{\mathbf{b}}} = \mathbf{M}_\mu\widehat{\mathbf{h}}, \quad \widehat{\widehat{\mathbf{j}}} = \mathbf{M}_\kappa\widehat{\mathbf{e}} \tag{7}$$

with the discrete permittivity matrix $\mathbf{M}_\varepsilon$, the permeability matrix $\mathbf{M}_\mu$, and the conductivity matrix $\mathbf{M}_\kappa$. In the case of cylindrical grids (or, generally speaking, if the primary and the dual grid are orthogonal) all material operators can be defined as diagonal matrices and thus are trivially symmetric positive (semi)definite. Note that the material matrices contain both averaged material parameters and the lengths and areas of the grid edges and faces, respectively.

The complete set of Eqs. (6) and (7) is referred to as *Maxwell's grid equations* and the corresponding *discrete material equations*.

One of the most important properties, relating the base mesh curl operator $\mathbf{C}$ and the dual mesh curl $\tilde{\mathbf{C}}$ operator, is the generalized symmetry

$$\tilde{\mathbf{C}} = \mathbf{C}^T. \tag{8}$$

It follows directly from the duality of the pair of staggered meshes and can be easily proven by simple topological considerations. However, this property is of outstanding importance if these topological matrices are used as discrete curl-operators as in FIT, as we will show below.

From the topology of each the primary and the dual grid we have a second set of properties [2,7,8],

$$\mathbf{SC} = \mathbf{0} \quad \text{and} \quad \tilde{\mathbf{S}}\tilde{\mathbf{C}} = 0, \tag{9}$$

which in the context of FIT can be interpreted as a discrete analogues to the vector-identity div curl = 0. Eq. (9) can be applied to prove many theorems concerning discrete electric and magnetic charges, as for example the discrete continuity equation.

Finally we can define a discrete *grad operator* $\mathbf{G}$ with the properties

$$\mathbf{G} = -\tilde{\mathbf{S}}^T \quad \text{and} \quad \tilde{\mathbf{G}} = -\mathbf{S}^T. \tag{10}$$

From (9) and (10) we obtain $\mathbf{CG} = \mathbf{0}$ and $\tilde{\mathbf{C}}\tilde{\mathbf{G}} = \mathbf{0}$, the discrete analogues to curl grad = 0. Eqs. (8)–(10) together with the symmetry of the material matrices build the foundation of basically all further properties of the discrete Maxwell equations as derived by the finite integration technique.

In the stability analysis we start with the *time-continuous* and *space-discrete* version of the discretization method (for the lossless case with $\mathbf{M}_\kappa = 0$):

$$\mathbf{C}\widehat{\mathbf{e}} = -\frac{\mathrm{d}}{\mathrm{d}t}\mathbf{M}_\mu\widehat{\mathbf{h}}, \quad \tilde{\mathbf{C}}\widehat{\mathbf{h}} = \frac{\mathrm{d}}{\mathrm{d}t}\mathbf{M}_\varepsilon\widehat{\mathbf{e}}, \;\rightarrow\; \mathbf{M}_\varepsilon^{-1}\tilde{\mathbf{C}}\mathbf{M}_\mu^{-1}\mathbf{C}\widehat{\mathbf{e}} = -\frac{\mathrm{d}^2}{\mathrm{d}t^2}\widehat{\mathbf{e}}.$$

Using (8) and the squareroots $\mathbf{M}_\varepsilon^{-1} = \mathbf{M}_\varepsilon^{-1/2}\mathbf{M}_\varepsilon^{-1/2}$, $\mathbf{M}_\mu^{-1} = \mathbf{M}_\mu^{-1/2}\mathbf{M}_\mu^{-1/2}$ of the (symmetric positive definite) material matrices, the system matrix of this eigenvalue equation can be transformed into

$$\mathbf{M}_\varepsilon^{-1}\tilde{\mathbf{C}}\mathbf{M}_\mu^{-1}\mathbf{C} = \mathbf{M}_\varepsilon^{-1/2}\left(\mathbf{M}_\mu^{-1/2}\mathbf{C}\mathbf{M}_\varepsilon^{-1/2}\right)^T\left(\mathbf{M}_\mu^{-1/2}\mathbf{C}\mathbf{M}_\varepsilon^{-1/2}\right)\mathbf{M}_\varepsilon^{1/2},$$

and thus has only real and non-negative eigenvalues λ_i. That means that all eigensolutions of the spatial discretization scheme expressed by this system matrix correspond to non-dissipative and non-growing oscillations with a real-valued circular frequency $\omega_i = \sqrt{\lambda_i}$ and the time-dependency $\widehat{\mathbf{e}}(t) \propto \mathrm{Re}\{\mathrm{e}^{j\omega_i t}\}$.

This is the proof for the *space stability* of the time-continuous formulation of the Maxwell's grid equations. The next step in the stability analysis for the complete time domain algorithm is the stability of the time-stepping scheme applied to this system.

In the *time-continuous* regime of our discretization as performed so far the vector potential and the scattered field approach in (2) and (3) can be easily adopted by

$$\widehat{\mathbf{h}}^{\mathrm{sc}} = \widehat{\mathbf{h}} - \widehat{\mathbf{h}}^0 = \frac{\mathrm{d}}{\mathrm{d}t}\widehat{\mathbf{a}}, \quad \widehat{\mathbf{a}}(t) = \int_{-\infty}^{t} \widehat{\mathbf{h}}^{\mathrm{sc}}(\tau)\,\mathrm{d}\tau, \tag{11}$$

where $\widehat{\mathbf{a}}$ is a *discrete vector potential*.

Like finite difference schemes, the FIT allows the implementation of a moving-mesh approach [9]. Due to causality reasons, no fields can ever precede the first particle of the bunch. A particle at any set position within or behind the bunch will never be affected by anything that happens behind it, and thus these fields need not to be computed. Reducing the numerical cost (both storage and CPU-time) significantly, the moving mesh approach allows us to simulate very long structures. As a consequence, we can solve for the wake fields of much shorter bunches than with the static mesh.

In the standard case of a staircase approximation of the boundary the results using a moving mesh are fully equivalent to a stationary mesh, as no interpolation is necessary. An important prerequisite, however,

is the usage of the 'magic' time step $c\Delta t = \Delta z$ which is adapted to the velocity $v = c$ of the bunch. This may come into conflict with the stability constraints of the time integration and will be analyzed below.

4. Implicit scheme

In the following we are interested in the situation when the longitudinal dimension (z-dimension) of the domain Ω is infinite or much longer than the transverse size of the domain. This situation is typical in accelerator applications and forces us to look for a scheme with preferable dispersion property in the longitudinal direction.

To establish an implicit time-stepping algorithm we can approximate the time derivatives in (6) by central difference expressions with $\widehat{\mathbf{h}}^n = \widehat{\mathbf{h}}(t_n)$ and $t_n = t_0 + n\Delta t$:

$$\begin{aligned}
&\widehat{\mathbf{h}}^{n+1} = \widehat{\mathbf{h}}^n - \Delta t \mathbf{M}_{\mu^{-1}} \mathbf{C} \widehat{\mathbf{e}}^{n+1/2}, \quad \widehat{\mathbf{e}}^{n+1/2} = \widehat{\mathbf{e}}^{n-1/2} + \Delta t \mathbf{M}_{\varepsilon^{-1}} \left(\mathbf{C}_1^T \bar{\widehat{\mathbf{h}}}^n + \mathbf{C}_2^T \widehat{\mathbf{h}}^n - \widehat{\mathbf{j}}^n \right), \\
&\bar{\widehat{\mathbf{h}}}^n \equiv \theta \widehat{\mathbf{h}}^{n+1} + (1 - 2\theta) \widehat{\mathbf{h}}^n + \theta \widehat{\mathbf{h}}^{n-1},
\end{aligned} \tag{12}$$

where we have split the discrete curl operator $\tilde{\mathbf{C}} = \mathbf{C}^T$ into the transversal operator $\mathbf{C}_1^T$ and the longitudinal operator $\mathbf{C}_2^T$, and θ is a numerical parameter to be defined. For our cylindrical $\{z, r, \varphi\}$-grid the operators have the form

$$\mathbf{C}_1 = \begin{pmatrix} \mathbf{0} & -\mathbf{P}_\varphi & \mathbf{P}_r \\ \mathbf{P}_\varphi & \mathbf{0} & \mathbf{0} \\ -\mathbf{P}_r & \mathbf{0} & \mathbf{0} \end{pmatrix}, \quad \mathbf{C}_2 = \begin{pmatrix} \mathbf{0} & \mathbf{0} & \mathbf{0} \\ \mathbf{0} & \mathbf{0} & -\mathbf{P}_z \\ \mathbf{0} & \mathbf{P}_z & \mathbf{0} \end{pmatrix}.$$

As easy to see the scheme (12) differs from the conventional "leap-frog" scheme [10] by usage of averaged value $\bar{\widehat{\mathbf{h}}}^n$ in the second relation. This "trick" changes the dispersion relation and the stability condition of the scheme as required and described below.

From Eqs. (11) and (12) we obtain an implicit three level numerical scheme for the vector potential $\widehat{\mathbf{a}}^n$:

$$\begin{aligned}
&(\mathbf{I} + \theta \mathbf{T}) \widehat{\mathbf{a}}^{n+1} = 2\widehat{\mathbf{a}}^n - \widehat{\mathbf{a}}^{n-1} - \mathbf{T}\left((1 - 2\theta) \widehat{\mathbf{a}}^n + \theta \widehat{\mathbf{a}}^{n-1} \right) - \mathbf{L} \widehat{\mathbf{a}}^n + \widehat{\mathbf{f}}^n, \\
&\mathbf{T} = \Delta t^2 \mathbf{M}_{\mu^{-1}} \mathbf{C} \mathbf{M}_{\varepsilon^{-1}} \mathbf{C}_1^T, \quad \mathbf{L} = \Delta t^2 \mathbf{M}_{\mu^{-1}} \mathbf{C} \mathbf{M}_{\varepsilon^{-1}} \mathbf{C}_2^T, \\
&\widehat{\mathbf{f}}^n = -(\mathbf{I} + \theta \mathbf{T}) \widehat{\mathbf{a}}_0^{n+1} + 2\widehat{\mathbf{a}}_0^n - \widehat{\mathbf{a}}_0^{n-1} - \mathbf{T}\left((1 - 2\theta) \widehat{\mathbf{a}}_0^n + \theta \widehat{\mathbf{a}}_0^{n-1} \right) - \mathbf{L} \widehat{\mathbf{a}}_0^n, \\
&\widehat{\mathbf{a}}_0^n = \int_{-\infty}^{t_n} \widehat{\mathbf{h}}_0 \, \mathrm{d}\tau.
\end{aligned} \tag{13}$$

This scheme approximates the problem (4). The local approximation error in homogeneous parts of the domain Ω is of second order in space and time $\mathrm{O}(\|\Delta h\|^2 + \Delta t^2)$, $\Delta h = (\Delta z, \Delta r, \Delta \varphi)$. The global approximation error and the rate of convergence depend critically on the approximation of material interfaces (boundary conditions) and will be considered later. For vacuum domains Ω the vector $\widehat{\mathbf{f}}^n$ approximates only the boundary conditions on $\partial\Omega$, and its components corresponding to cells inside Ω are equal to zero. The relations (13) are defined on dual grid complexes, which cover the domain Ω and usually contain cells which do not belong to the domain Ω. To install the updating Eq. (12) on the complete dual grid complexes we use a modification of the entries of the material matrices $\mathbf{M}_{\varepsilon^{-1}}, \mathbf{M}_{\mu^{-1}}$ conserving their symmetry and positive semi-definiteness as described in the following sections.

In the above relations the vector $\widehat{\mathbf{a}}_0^n$ is presented as an improper time integral of the magnetic field of a relativistic bunch in free space [1]. It is geometry free and depends only on the longitudinal charge distribution $\lambda(z-ct)$ (see relation (15)). Hence, it has to be calculated only once at the beginning of the simulation. Since the charge distribution equal to zero at infinity the time integral can be avoided completely by using the relation

$$\frac{\partial}{\partial z}\vec{A}^0(z-ct) = -\frac{1}{c}\frac{\partial}{\partial t}\vec{A}^0(z-ct), \quad \vec{A}^0(z-ct) = \int_{-\infty}^{t} \vec{H}^0(z-c\tau)\,\mathrm{d}\tau,$$

which allows to convert the space derivative to a time derivative.

From the results of the previous section it follows that all eigensolutions of the spatial discretization correspond to non-dissipative and non-growing oscillations that ensure the late time stability of the scheme. The next step is the stability of the time-stepping scheme. Our scheme is implicit in the transversal plane and explicit in z-direction. From a Fourier stability analysis a sufficient spectral stability condition in free space can easily be obtained

$$c\Delta t \leqslant \Delta z, \quad 0.25 \leqslant \theta, \tag{14}$$

combining two conditions: first, the stability condition of the explicit scheme for the one-dimensional (longitudinal) wave equation, and second the stability condition for the weighted implicit three level scheme. Note, that the condition (14) does not take into account approximation of boundary conditions.

With the time step $c\Delta t = \Delta z$ allowed by condition (14) the scheme (13) has no dispersion in the longitudinal direction (in analogy to explicit schemes for the one-dimensional wave equation [10]) and a moving mesh can be employed easily [9].

To reduce the dispersion in the transversal direction we should use the minimal value of θ. Due to the fact that the transverse dimensions of the domain Ω are much smaller than the longitudinal one, the zero dispersion property in the direction of the motion allows for a non-deteriorating calculation of the solution for as long as necessary. This has been confirmed by numerical examples (see also [4]).

5. Staircase realization for rotationally symmetric geometry

In this section we describe the realization of the scheme for the case of a rotationally symmetric geometry in a standard staircase approximation of the boundary, which can be realized by diagonal material matrices $\mathbf{M}_{\mu^{-1}}, \mathbf{M}_{\varepsilon^{-1}}$.

In the staircase approximation the domain Ω is approximated by the cell complex $\Omega_h \subseteq K$, and the matrices $\mathbf{M}_{\varepsilon^{-1}}, \mathbf{M}_{\mu^{-1}}$ are diagonal ones with the elements (without double indices for simplicity of notation)

$$(\hat{\varepsilon}_{pijk})^{-1} = \begin{cases} \left(\varepsilon\frac{\tilde{S}_{pijk}}{L_{pijk}}\right)^{-1} & \text{if } L_{pijk} \in \Omega_h \setminus \partial\Omega_h, \\ 0 & \text{if } L_{pijk} \notin \Omega_h \setminus \partial\Omega_h, \end{cases}$$

$$(\hat{\mu}_{pijk})^{-1} = \begin{cases} \left(\mu\frac{S_{pijk}}{\tilde{L}_{pijk}}\right)^{-1} & \text{if } S_{pij} \in \Omega_h \setminus \partial\Omega_h, \\ 0 & \text{if } S_{pijk} \notin \Omega_h \setminus \partial\Omega_h, \end{cases}$$

with $i = 1,\ldots,N_z$, $j = 1,\ldots,N_r$, $k = 1,\ldots,N_\varphi$, $p = z, r, \varphi$ and the face areas and edge lengths of the primary and secondary grid $S, L, \tilde{S}, \tilde{L}$, respectively.

For a bunch moving at speed of light c with an offset a from and parallel to the axis of a rotationally symmetric structure, the source current $\vec{j}$ can be represented as

$$\vec{j} = \frac{\vec{c}\lambda(z/c - t)\delta(r - a)}{\pi a} \sum_{m=0}^{\infty} \frac{\cos m\varphi}{1 + \delta_{m0}}, \tag{15}$$

where $\lambda(s)$ is the longitudinal charge distribution and m is the azimuthal mode number.

The numerical scheme (13) for an azimuthal mode number m has the form

$$\begin{aligned}
&-\mathbf{M}_{\mu_z^{-1}}^{-1}\Delta t^{-2}\left(\widehat{\mathbf{a}}_z^{n+1} - 2\widehat{\mathbf{a}}_z^{n} + \widehat{\mathbf{a}}_z^{n-1}\right) = m\mathbf{M}_{\varepsilon_r^{-1}}\mathbf{P}_z^T\widehat{\mathbf{a}}_\varphi^n - \mathbf{P}_r\mathbf{M}_{\varepsilon_\varphi^{-1}}\mathbf{P}_z^T\widehat{\mathbf{a}}_r^n + \left(\mathbf{P}_r\mathbf{M}_{\varepsilon_\varphi^{-1}}\mathbf{P}_r^T + m^2\mathbf{M}_{\varepsilon_r^{-1}}\right)\bar{\widehat{\mathbf{a}}}_z^n - \widehat{\mathbf{f}}_z^n,\\
&-\mathbf{M}_{\mu_r^{-1}}^{-1}\Delta t^{-2}\left(\widehat{\mathbf{a}}_r^{n+1} - 2\widehat{\mathbf{a}}_r^{n} + \widehat{\mathbf{a}}_r^{n-1}\right) = \mathbf{P}_z\mathbf{M}_{\varepsilon_\varphi^{-1}}\mathbf{P}_z^T\widehat{\mathbf{a}}_r^n + \left(m^2\mathbf{M}_{\varepsilon_z^{-1}}\bar{\widehat{\mathbf{a}}}_r^n - \mathbf{P}_z\mathbf{M}_{\varepsilon_\varphi^{-1}}\mathbf{P}_r^T\bar{\widehat{\mathbf{a}}}_z^n + m\mathbf{M}_{\varepsilon_z^{-1}}\mathbf{P}_r^T\bar{\widehat{\mathbf{a}}}_\varphi^n\right) - \widehat{\mathbf{f}}_r^n,\\
&-\mathbf{M}_{\mu_\varphi^{-1}}^{-1}\Delta t^{-2}\left(\widehat{\mathbf{a}}_\varphi^{n+1} - 2\widehat{\mathbf{a}}_\varphi^{n} + \widehat{\mathbf{a}}_\varphi^{n-1}\right) = \mathbf{P}_z\mathbf{M}_{\varepsilon_r^{-1}}\mathbf{P}_z^T\widehat{\mathbf{a}}_\varphi^n + \left(\mathbf{P}_r\mathbf{M}_{\varepsilon_z^{-1}}\mathbf{P}_r^T\bar{\widehat{\mathbf{a}}}_\varphi^n + m\mathbf{P}_z\mathbf{M}_{\varepsilon_r^{-1}}\bar{\widehat{\mathbf{a}}}_z^n + m\mathbf{P}_r\mathbf{M}_{\varepsilon_z^{-1}}\bar{\widehat{\mathbf{a}}}_r^n\right) - \widehat{\mathbf{f}}_\varphi^n,
\end{aligned} \tag{16}$$

where $\bar{\widehat{\mathbf{a}}}_p^n \equiv \theta\widehat{\mathbf{a}}_p^{n+1} + (1 - 2\theta)\widehat{\mathbf{a}}_p^n + \theta\widehat{\mathbf{a}}_p^{n-1}$, $p = r, \varphi, z$, and we used the fact that $P_\varphi = mI$ [11].

When a bunch moves along the axis, only the $\vec{A}_\varphi$ component of vector potential is different from zero and our scheme with $\theta = 0.5$ is reduced to the staircase scheme of the paper [12].

The material matrices $\mathbf{M}_{\mu^{-1}}, \mathbf{M}_{\varepsilon^{-1}}$ in a staircase approximation of the geometry are diagonal and for higher order modes it is possible to use the divergence relation

$$\widehat{\mathbf{a}}_\varphi = m^{-1}\mathbf{M}_{\mu_\varphi^{-1}}\left(\mathbf{P}_r\mathbf{M}_{\mu_r^{-1}}^{-1}(\widehat{\mathbf{a}}_r + \widehat{\mathbf{a}}_r^0) + \mathbf{P}_z\mathbf{M}_{\mu_z^{-1}}^{-1}(\widehat{\mathbf{a}}_z + \widehat{\mathbf{a}}_z^0)\right) - \widehat{\mathbf{a}}_\varphi^0 \tag{17}$$

to eliminate the $\mathbf{a}_\varphi$ component from the equations for the $\mathbf{a}_r, \mathbf{a}_z$ components:

$$\begin{aligned}
&-\mathbf{M}_{\mu_r^{-1}}^{-1}\Delta t^{-2}\left(\widehat{\mathbf{a}}_r^{n+1} - 2\widehat{\mathbf{a}}_r^{n} + \widehat{\mathbf{a}}_r^{n-1}\right) = \mathbf{P}_z\mathbf{M}_{\varepsilon_\varphi^{-1}}\mathbf{P}_z^T\widehat{\mathbf{a}}_r^n + \Big((\mathbf{M}_{\varepsilon_z^{-1}}\mathbf{P}_r^T\mathbf{M}_{\mu_\varphi^{-1}}\mathbf{P}_r\mathbf{M}_{\mu_r^{-1}}^{-1} + m^2\mathbf{M}_{\varepsilon_z^{-1}})\bar{\widehat{\mathbf{a}}}_r^n\\
&\quad + (\mathbf{M}_{\varepsilon_z^{-1}}\mathbf{P}_r^T\mathbf{M}_{\mu_\varphi^{-1}}\mathbf{P}_z\mathbf{M}_{\mu_z^{-1}}^{-1} - \mathbf{P}_z\mathbf{M}_{\varepsilon_\varphi^{-1}}\mathbf{P}_r^T)\bar{\widehat{\mathbf{a}}}_z^n\Big) - \widehat{\mathbf{f}}_r'^n,\\
&-\mathbf{M}_{\mu_z^{-1}}^{-1}\Delta t^{-2}\left(\widehat{\mathbf{a}}_z^{n+1} - 2\widehat{\mathbf{a}}_z^{n} + \widehat{\mathbf{a}}_z^{n-1}\right) = \mathbf{M}_{\varepsilon_r^{-1}}\mathbf{P}_z^T\mathbf{M}_{\mu_\varphi^{-1}}\mathbf{P}_z\mathbf{M}_{\mu_z^{-1}}^{-1}\widehat{\mathbf{a}}_z^n + (\mathbf{M}_{\varepsilon_r^{-1}}\mathbf{P}_z^T\mathbf{M}_{\mu_\varphi^{-1}}\mathbf{P}_r\mathbf{M}_{\mu_r^{-1}}^{-1}\\
&\quad - \mathbf{P}_r\mathbf{M}_{\varepsilon_\varphi^{-1}}\mathbf{P}_z^T)\widehat{\mathbf{a}}_r^n + (\mathbf{P}_r\mathbf{M}_{\varepsilon_\varphi^{-1}}\mathbf{P}_r^T + m^2\mathbf{M}_{\varepsilon_r^{-1}})\bar{\widehat{\mathbf{a}}}_z^n - \widehat{\mathbf{f}}_z'^n.
\end{aligned} \tag{18}$$

The system (18) does not contain static solutions and its dimension is reduced by 1/3 in its rank. It can be solved easily. At the first step we calculate the vector $\widehat{\mathbf{a}}_z^{n+1}$ and have to solve a linear system with the matrix $\mathbf{I} + \Delta t^2\theta\mathbf{M}_{\mu_z^{-1}}\mathbf{P}_r\mathbf{M}_{\varepsilon_\varphi^{-1}}\mathbf{P}_r^T + m^2\Delta t^2\theta\mathbf{M}_{\mu_z^{-1}}\mathbf{M}_{\varepsilon_r^{-1}}$. This matrix is a block diagonal one with N_z blocks. Each block is a three-banded matrix of size N_r and can be resolved by $\mathrm{O}(N_r)$ operation. Now we can use the component $\widehat{\mathbf{a}}_z^{n+1}$ in the equation for the component $\widehat{\mathbf{a}}_r^{n+1}$ and have to solve a linear system with the matrix $\mathbf{I} + \Delta t^2\theta\mathbf{M}_{\mu_r^{-1}}\mathbf{M}_{\varepsilon_z^{-1}}\mathbf{P}_r^T\mathbf{M}_{\mu_\varphi^{-1}}\mathbf{P}_r\mathbf{M}_{\mu_r^{-1}}^{-1} + m^2\Delta t^2\theta\mathbf{M}_{\mu_r^{-1}}\mathbf{M}_{\varepsilon_z^{-1}}$. This matrix is again a block diagonal one with N_z blocks. Each block is also a three-banded matrix of size N_r and can be resolved by an $\mathrm{O}(N_r)$ operation.

The above consideration shows that the implicit solution of the system (18) requires only $\mathrm{O}(N_rN_z)$ operations, and the numerical complexity of the new algorithm is of the same order of operations as the explicit FIT/FDTD method used in codes like TBCI [13], MAFIA [7].

6. Second order convergent scheme

With the standard staircase approximation of curved boundaries we will not obtain a second order scheme in the general case. To develop a second order convergent scheme in the L_2^h grid norm we adopt the

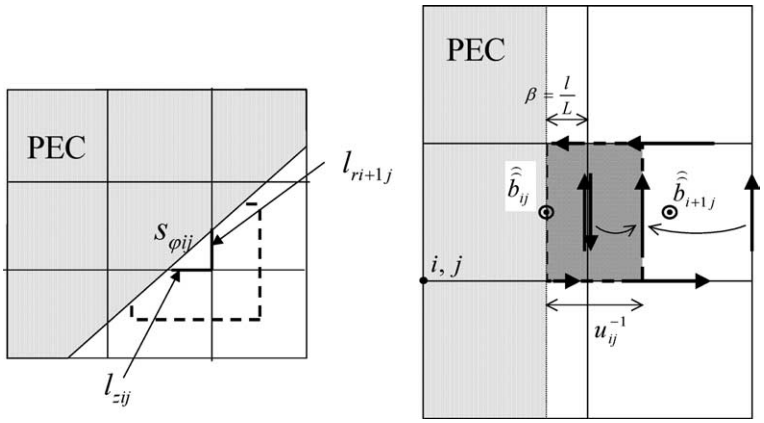

Fig. 2. Curved PEC-boundary in Cartesian mesh.

approach of the paper [5], where a new conformal scheme for explicit FDTD algorithm was constructed and its second order convergence was proven analytically and by numerical experiments. It was also shown numerically that unlike the scheme derived in [14] the new scheme is stable without the need to reduce the maximum stable time step due to small "cut" cells near the boundary.

In the conformal approach we allow the cells of the grid to be only *partially filled* by a perfectly electric conducting (PEC) material with an arbitrarily shaped interface. Since the area of the cells near the boundary is reduced, the time step in the conformal scheme [14] has to be reduced, too.

Consider Fig. 2(left). To calculate the flux $\hat{\hat{b}}_{\varphi ijk}$ in standard conformal schemes only the non-zero voltages $\hat{e}_{ri+1jk}$ and $\hat{e}_{zijk}$ are used. Apparently, this information is not sufficient to do the same "big" time step in this small cell, which we can use for cells inside the calculation domain. The idea of the method presented here is to use also the information from the adjacent cells to enlarge the local curl-operation and thus to enable the usage of the same time step as before.

To this end, we will build an approximation of the *virtual cell* shown by the dashed line in Fig. 2(left), which is realized by non-diagonal elements in the material matrix $\mathbf{M}_{\mu^{-1}}$ *for boundary cells only*. This means, that inside the domain we can still use the conventional FIT algorithm. The update equations of the electric components will not be changed at all compared to standard conformal scheme [14].

As a consequence, only the material matrix $\mathbf{M}_{\mu^{-1}}$ of the algorithm described in [5] has to be modified to derive the stable algorithm without reducing the time step. The original material matrix $\mathbf{M}_{\mu^{-1}}$ is a composition of diagonal matrices: $\mathbf{M}_{\mu^{-1}} = \tilde{\mathbf{R}}\mathbf{M}$, $\mathbf{M} = \|\mu_{pijk}^{-1}\|$, $\tilde{\mathbf{R}} = \|\tilde{r}_{pijk}^{-1}\|$, $\underset{\sim}{\mu}_{pijk} = \mu s_{pijk}/S_{pijk}$, $\tilde{r}_{pijk} = S_{pijk}/\tilde{L}_{pijk}$, where s denotes a reduced cell area [5]. A new material matrix $\tilde{\mathbf{M}}_{\mu^{-1}}$ is composed by the relation $\tilde{\mathbf{M}}_{\mu^{-1}} = \mathbf{V}^T\mathbf{D}\mathbf{V}$, where $\mathbf{D} = \tilde{\mathbf{R}}\mathbf{U} > 0$ is a diagonal matrix, responsible for the order of the approximation, and $\mathbf{V}$ is a non-diagonal matrix of weights. In [5] we described the construction of the matrix $\tilde{\mathbf{M}}_{\mu^{-1}}$ for an explicit algorithm. Since the scheme here is implicit in the transversal direction we use the weights only in longitudinal direction and only for facets in zr and $z\varphi$ planes.

In the following we will consider the domain Ω with the material parameters of free space $\mu = 1, \varepsilon = 1$ and decomposed by equidistant grid complex with the mesh parameter $L = L_{rijk} = L_{zijk}$.

To simplify the notation, we consider only one the zr-plane and omit the index k for the φ-direction. At first we will build an auxiliary matrix $\mathbf{V}^0$:

$$v^0_{\varphi ij,\varphi ij} = 1(\boxplus);$$
$$v^0_{\varphi ij,\varphi i+1j} = \max(0, a - \mu_{\varphi ij}\varepsilon_{ri+1j})(\boxplus); \quad v^0_{\varphi ij,\varphi i-1j} = \max(0, a - \mu_{\varphi ij}\varepsilon_{rij})(\boxplus).$$

Here, a is a constant parameter equal to 0.99 [5]. It follows from the relations above that only cells near the boundary will give a contribution to non-diagonal elements of the matrix $\mathbf{V}^0$.

From the matrix $\mathbf{V}^0$ we will build a matrix $\mathbf{V}$:

$$v_{\varphi ij,\varphi i_1 j_1} = v^0_{\varphi ij,\varphi i_1 j_1} \Big/ \sum_{i_2 j_2} v^0_{\varphi i_2 j_2,\varphi i_1 j_1}., \tag{19}$$

where the sum is taken over all elements of the corresponding column.

The diagonal matrix $\mathbf{U}$ has elements

$$u_{\varphi ij} = \left(\sum_{i_1 j_1} v_{\varphi ij,zi_1 j_1} \mu_{\varphi i_1 j_1} \right)^{-1}, \tag{20}$$

where the sum is taken over all elements of the corresponding row.

For a geometric interpretation of the weights defined by this procedure we consider the simple case in Fig. 2(right), where the interface to the PEC material is parallel to the $r\varphi$-coordinate plane, with a vacuum to PEC-ratio of $\beta < a$. This leads to

$$\mu_{\varphi ij} = \varepsilon_{zij} = \varepsilon_{zij+1} = \beta, \quad \varepsilon_{ri+1j} = \varepsilon_{ri+2j} = \varepsilon_{zi+1j} = \varepsilon_{zi+1j+1} = 1,$$

and all entries of the corresponding row of $\mathbf{V}^0$ are zero except for $v^0_{\varphi ij,\varphi i+1j} = a - \beta$. From (19) and (20) we obtain

$$v_{\varphi ij,\varphi i+1j} = \frac{a-\beta}{1+a-\beta}, \quad v_{\varphi ij,\varphi ij} = 1, \quad u_{\varphi ij} = \frac{1}{\beta + v_{\varphi ij,\varphi i+1j}}.$$

Returning to Fig. 2(right), and remembering that each of the magnetic flux-components involved is calculated by a local curl of electric voltages, we can now see, that this weighting procedure is indeed equivalent to a local curl around the virtual cell with step size $u^{-1}_{\varphi ij}$ using interpolated electric voltages. Finally the obtained flux is correlated with the enlarged area of this virtual cell to transform it in a magnetic voltage.

A similar, but more complicated geometric interpretation is possible also for the general case (of arbitrarily shaped interface planes), and again it can be shown, that our formulas define interpolated local curls referring to virtual cells.

Relations (19) and (20) allow us to derive (see [5]) the order of the local approximation error in the material relations. We consider again the situation when only the weight $v_{\varphi ij,\varphi i+1j}$ for one adjacent cell is unequal to zero,

$$\begin{aligned} &\tilde{\mathbf{M}}_{\mu^{-1}} = \mathbf{V}^* \tilde{\mathbf{R}} \mathbf{U} \mathbf{V}, \\ &(\tilde{\mathbf{R}} \mathbf{U} \mathbf{V} b)_{\varphi ij} = \frac{\hat{\hat{b}}_{\varphi ij} v_{\varphi ij,\varphi ij} + \hat{\hat{b}}_{\varphi i+1j} v_{\varphi ij,\varphi i+1j}}{\hat{\mu}_{\varphi ij} v_{\varphi ij,\varphi ij} + \hat{\mu}_{\varphi i+1j} v_{\varphi ij,\varphi i+1j}} = \hat{h}_{\varphi ij} + \mathrm{O}(L^2), \\ &(\tilde{\mathbf{M}}_{\mu^{-1}} b)_{\varphi ij} = \hat{h}_{\varphi ij} + \mathrm{O}(L^2). \end{aligned} \tag{21}$$

The last relation follows from (19), which means that the sum of all elements of any row of the matrix $\mathbf{V}^*$ is equal to one. Thus, we have at least a first order local approximation in the material relations near the boundary, and globally a second order convergent scheme in L^h_2 grid norm – if it is stable.

For spatial stability, it follows directly from (21) that the material matrix $\tilde{\mathbf{M}}_{\mu^{-1}}$ is symmetric and the matrix $\mathbf{A} = c^2 \tilde{\mathbf{M}}_{\mu^{-1}} \mathbf{C} \mathbf{M}_{\varepsilon^{-1}} \mathbf{C}^T$ has only real non-negative eigenvalues.

In our conformal scheme the material matrix $\tilde{\mathbf{M}}_{\mu_r^{-1}}$ is non-diagonal, which makes the usage of divergence relation (17) too expensive. For this reason we will describe next a modified approach based directly on the system (16).

In the first step we calculate the vector $\widehat{\mathbf{a}}_z^{n+1}$ and have to solve a linear system with the matrix $\mathbf{I}+\Delta t^2\theta\tilde{\mathbf{M}}_{\mu_z^{-1}}\mathbf{P}_r\mathbf{M}_{\varepsilon_j^{-1}}\mathbf{P}_r^T+m^2\Delta t^2\theta\tilde{\mathbf{M}}_{\mu_z^{-1}}\mathbf{M}_{\varepsilon_r^{-1}}$. Like in the staircase approximation this matrix in the conformal scheme is a block diagonal one with N_z blocks. Each block is a three-band matrix of size N_r and can be resolved by an $\mathrm{O}(N_r)$ operation.

Now we can use the component $\widehat{\mathbf{a}}_z^{n+1}$ in the equations for the components $\widehat{\mathbf{a}}_r^{n+1}$, $\widehat{\mathbf{a}}_\varphi^{n+1}$ which are coupled. We have to solve a system with the matrix

$$\begin{pmatrix} \mathbf{I}+\Delta t^2\theta m^2\tilde{\mathbf{M}}_{\mu_r^{-1}}\mathbf{M}_{\varepsilon_z^{-1}} & m\theta\tilde{\mathbf{M}}_{\mu_r^{-1}}\mathbf{M}_{\varepsilon_z^{-1}}\mathbf{P}_r^T \\ m\theta\tilde{\mathbf{M}}_{\mu_\varphi^{-1}}\mathbf{P}_r\mathbf{M}_{\varepsilon_z^{-1}} & \mathbf{I}+\Delta t^2\theta\tilde{\mathbf{M}}_{\mu_\varphi^{-1}}\mathbf{P}_r\mathbf{M}_{\varepsilon_z^{-1}}\mathbf{P}_r^T \end{pmatrix}, \tag{22}$$

which is a block diagonal one with N_z blocks.

Now as the first step we consider an algorithm for the case of diagonal material matrices (as it occurs in the staircase approximation) and then we show how to use this algorithm for the conformal scheme with non-diagonal material matrix $\tilde{\mathbf{M}}_{\mu_r^{-1}}$. In the case of diagonal matrix $\tilde{\mathbf{M}}_{\mu_r^{-1}}$ each block of matrix (22) is of size $2N_r$ and has a seven-banded structure as shown in Fig. 3. Each block can be reduced to a three diagonal type by an $\mathrm{O}(N_r)$ using Gauss elimination (see Fig. 3). This means its resolving takes only $\mathrm{O}(N_rN_z)$operations and the algorithm requires the same order of operations as the explicit FDTD method.

For the common case of non-diagonal matrix $\tilde{\mathbf{M}}_{\mu_r^{-1}}$ we use an iterative algorithm based on the splitting of the transversal operator $\mathbf{T}$. If we note by $\tilde{\mathbf{M}}^0_{\mu^{-1}}$ the diagonal part of the material matrix $\tilde{\mathbf{M}}_{\mu^{-1}}$, the iterative scheme reads

$$\begin{aligned} &(\mathbf{I}+\theta\mathbf{T}^0)(\widehat{\mathbf{a}}^{n+1})^i=\widehat{\mathbf{f}}''^n-\theta\mathbf{T}^1(\widehat{\mathbf{a}}^{n+1})^{i-1},\quad i=1,2,\ldots,\\ &\widehat{\mathbf{f}}''^n=\mathbf{T}((1-2\theta)\widehat{\mathbf{a}}^n+\theta\widehat{\mathbf{a}}^{n-1})+2\widehat{\mathbf{a}}^n-\widehat{\mathbf{a}}^{n-1}-\mathbf{L}\widehat{\mathbf{a}}^n+\widehat{\mathbf{f}}^n,\\ &\mathbf{T}^0=\Delta t^2\tilde{\mathbf{M}}^0_{\mu^{-1}}\mathbf{C}\mathbf{M}_{\varepsilon^{-1}}\mathbf{C}_1^T,\quad \mathbf{T}^1=\Delta t^2(\tilde{\mathbf{M}}_{\mu^{-1}}-\tilde{\mathbf{M}}^0_{\mu^{-1}})\mathbf{C}\mathbf{M}_{\varepsilon^{-1}}\mathbf{C}_1^T, \end{aligned} \tag{23}$$

where the operator $\mathbf{T}^1$ is of very low rank. As the start value of the unknown vector we use a solution of the system

$$(\mathbf{I}+\theta\mathbf{T}^0)\left(\widehat{\mathbf{a}}^{n+1}\right)^0=-\mathbf{T}^0\left((1-2\theta)\widehat{\mathbf{a}}^n+\theta\widehat{\mathbf{a}}^{n-1}\right)+2\widehat{\mathbf{a}}^n-\widehat{\mathbf{a}}^{n-1}-(\mathbf{T}^1+\mathbf{L})\widehat{\mathbf{a}}^n+\widehat{\mathbf{f}}^n. \tag{24}$$

Like (23), the expression (24) is an approximation of the problem (4) of order $\mathrm{O}(\|\Delta h\|^2+\Delta t^2)$, $\Delta h=(\Delta z,\Delta r)$, but unstable for $c\Delta t=\Delta z$. In all our numerical examples it was sufficient to perform one

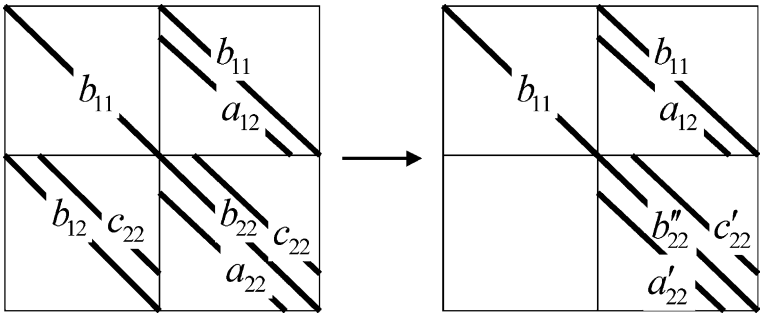

Fig. 3. Reduction of the matrix.

iteration step (23) to obtain a stable solution. For both Eqs. (23) and (24) we have to invert the matrix $\mathbf{I}+\theta\mathbf{T}^0$ and consequently the algorithm described above for a seven-band matrix can be applied.

In all examples shown in the next section we use the scheme (23) and (24) in combination with a moving mesh.

7. Indirect method for the calculation of the wake potential

For a bunch described by the source current (15) the longitudinal wake potential at mode m is defined by [13]

$$W_{\parallel}^{m}(r,s)=-\frac{1}{Q}\int_{-\infty}^{\infty}E_z^{\mathrm{sc}}(r,z,t(z,s))\,\mathrm{d}z,\quad Q=\int_{-\infty}^{\infty}\lambda(z)\,\mathrm{d}z, \tag{25}$$

where s is the distance behind a given origin $z_0=vt$ in the exciting bunch, and

$$t(z,s)=(z+s)/v.$$

As was shown in [16] the improper integral (25) for cavity-like structure can be reduced to a proper integral over the gap of the cavity. In [17] the above result was generalized by showing that the longitudinal and transverse wake potentials, at all orders m in the multi-polar expansion, can be expressed as integrals over the wake fields along any arbitrary contour spanning the structure longitudinally.

To calculate the wake potential $W_{\parallel}^{m}$ we use a modification of the indirect method described in [17].

The main feature of our method is that (like in the direct method) we integrate only the $\bar{e}_z(r,z,s)=E_z^{\mathrm{sc}}(r,z,t(z,s))$ component of the scattered electromagnetic field along a straight line L_{r_0} at radius r_0, and use other field components only at the end of the structure. Note, that in the original method [17] we have to integrate a linear combination of $\bar{e}_z^s$ and $\bar{b}_z^s$ components along L_{r_0}.

As it was shown in [17], for each mode m the differential forms

$$\omega_S=r^m[\bar{e}_r+c\bar{b}_\varphi-\bar{e}_\varphi+c\bar{b}_r]\mathrm{d}r+r^m[\bar{e}_z+c\bar{b}_z]\mathrm{d}z,$$
$$\omega_D=r^{-m}[\bar{e}_r+c\bar{b}_\varphi+\bar{e}_\varphi-c\bar{b}_r]\mathrm{d}r+r^{-m}[\bar{e}_z-c\bar{b}_z]\mathrm{d}z$$

are closed. Hence, we can write

$$QW_{\parallel}^{m}=-\int_{-\infty}^{\infty}\bar{e}_z\,\mathrm{d}z=-\int_{L_{r_0}}\bar{e}_z\,\mathrm{d}z-\int_{C_0}\bar{e}_z\,\mathrm{d}z,$$
$$\int_{C_0}\bar{e}_z\,\mathrm{d}z=-\frac{1}{2}\left(\int_{C_0}\left(r_0^m\omega_D+r_0^{-m}\omega_S\right)-\frac{\beta}{a^m}\int_{C_{15}}\omega_S\right),\quad \beta=\left(\frac{a}{r^0}\right)^m-\left(\frac{a}{r^0}\right)^{-m},\quad C_{15}=\bigcup_{i=1}^{5}C_i,$$

where a is the radius of the outgoing beam tube, and the other parameters are shown in Fig. 4. For a perfectly conducting geometry we easily obtain from the above relations:

$$\begin{aligned}\int_{C_0}\bar{e}_z\,\mathrm{d}z&=-\frac{1}{2}\left(\int_{C_1}\left(r_0^m\omega_D+r_0^{-m}\omega_S-\frac{\beta}{a^m}\omega_S\right)-\frac{\beta}{a^m}\int_{C_5}\omega_S\right)\\&=-\frac{1}{2}\int_0^{r_0}\beta(r/a)^m[\bar{e}_r+c\bar{b}_\varphi-\bar{e}_\varphi+c\bar{b}_r]\mathrm{d}r-\frac{1}{2}\int_{r_0}^{a}((r_0/r)^m+(r_0/r)^{-m}-\beta(r/a)^m)[\bar{e}_r+c\bar{b}_\varphi]\mathrm{d}r\\&\quad-\frac{1}{2}\int_{r_0}^{a}((r_0/r)^m-(r_0/r)^{-m}+\beta(r/a)^m)[\bar{e}_\varphi-c\bar{b}_r]\mathrm{d}r.\end{aligned}$$

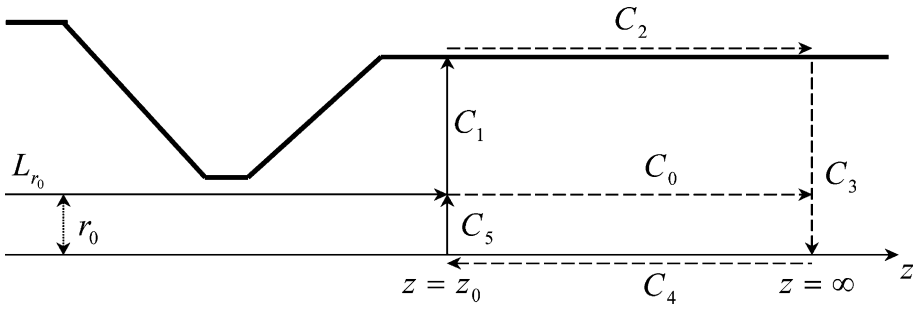

Fig. 4. Contours for the indirect integration.

Obviously the infinite contour C_0 can be replaced by the finite contours C_1, C_5. The transversal wake potential $W_\perp^m$ can be found from the longitudinal one by applying the Panowsky–Wenzel theorem [18].

In the following numerical examples we use integral parameters [15]: the loss factor $L_\parallel^m$ and the kick factor $L_\perp^m$ given by formulas

$$L_\parallel^m = \int_{-\infty}^{\infty} W_\parallel^m(s)\lambda(s)\,\mathrm{d}s, \quad L_\perp^m = \int_{-\infty}^{\infty} W_\perp^m(s)\lambda(s)\,\mathrm{d}s.$$

8. Numerical examples

Finally we discuss the results of numerical computations for several test problems. The new algorithm has been implemented in a code called ECHO.

Fig. 5 shows the relative error of the loss factor $\delta = |L_\parallel^0 - \bar{L}_\parallel^0|/\bar{L}_\parallel^0$ for a Gaussian bunch with RMS $\sigma = 0.5$ cm passing through a pillbox (Fig. 5 left) and a spherical resonator (Fig. 5 right). The error is given over the number of mesh steps per bunch length σ/h, where h denotes the equal mesh step $h = \Delta z = \Delta r$ in both directions. The pillbox has the length 1.8 cm and radius 0.9 cm. The sphere has the diameter 1.8 cm. The analytical loss factor $\bar{L}_\parallel^0$ is equal to $0.589459V/pC$ for the pillbox and $0.152446V/pC$ for the sphere. The error for a computation with a stationary mesh is demonstrated by lines. The results for the moving mesh

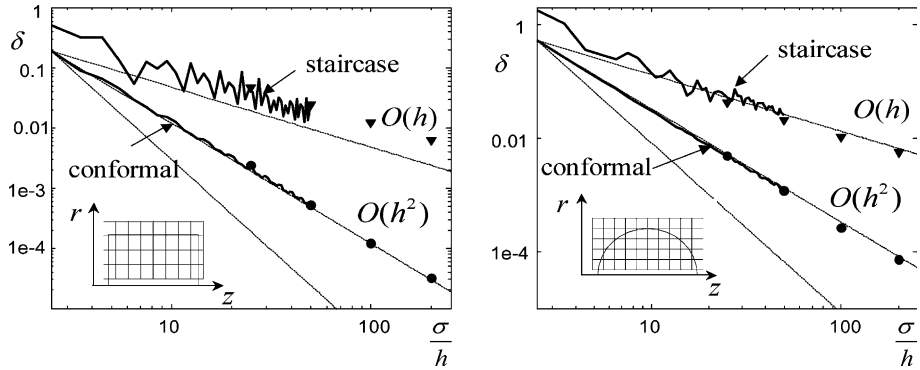

Fig. 5. The relative error of monopole loss factor for a pillbox (left) and a sphere (right) vs. number of mesh steps per RMS bunch length. The solid lines show results for a stationary mesh, the triangles and circles present results for the moving mesh.

are shown by triangles and circles. The moving mesh in this and the following examples, except the last one in Fig. 10, covers the Gaussian bunch longitudinally in the range from -5σ to 5σ. As expected, the staircase scheme shows a first order rate of convergence and the conformal scheme achieves the second order. Note, that in the pillbox example the mesh was not fitted to the boundary surface as in that case the conformal and staircase approximations would coincide.

As a next test example we use a circular collimator structure shown in Fig. 6 (with inner radius b not presented in the figure). Fig. 7 demonstrates the wake potential for the collimator with parameters $a = 40$ mm, $b = c = 10$ mm, $L = 2445$ mm and the bunch with RMS length $\sigma = 0.1$ cm. The solution is compared to the analytical estimation [19].

The conformal scheme shows a second order convergence and gives results of high accuracy with only 5 mesh steps per σ in all tests. Note that the staircase scheme with 5 steps per σ leads to an relative error in excess of 300%.

Next, we show results for the dipole wake ($m = 1$) and compare ECHO to results obtained by ABCI [20] (finite difference time domain method with triangular approximation of the boundary). In the following numerical examples we use $a = 35$ mm and $b = c = 2$ mm, where b is an interior radius of the collimator.

In Fig. 8(left) the transversal dipole loss factor $L_{\perp}^{1}$ for the collimator with $L = 10$ cm is shown for different mesh resolutions σ/h, where $\sigma = 1$ mm for the Gaussian bunch and h is the mesh step. The error compared to the reference value (finest mesh resolution) is also shown in the figure. The dashed lines show

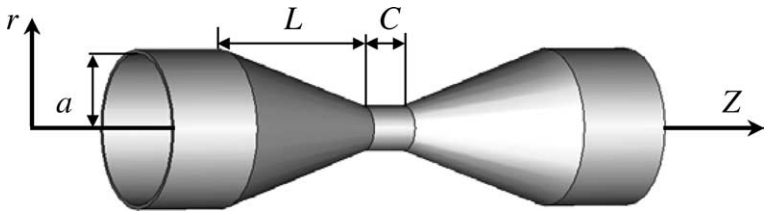

Fig. 6. The geometry of the collimator.

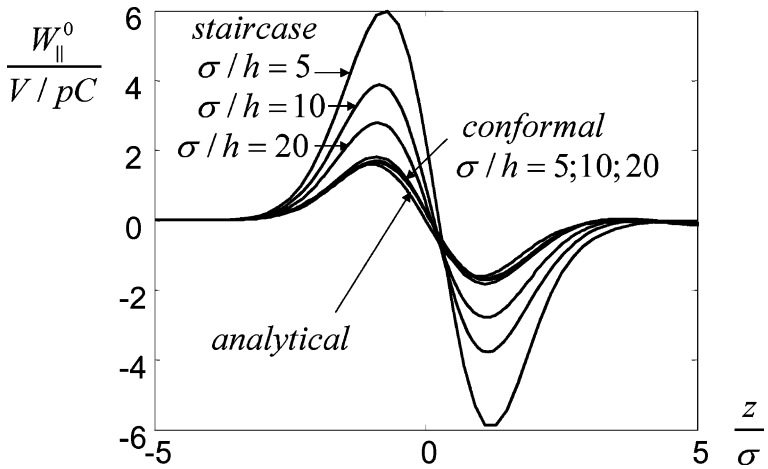

Fig. 7. The monopole wake potential of a collimator. The wakes calculated with different mesh resolutions σ/h are compared to the analytical estimation. The results for the staircase scheme show a considerable error. Three curves for the conformal scheme follow the analytical estimation.

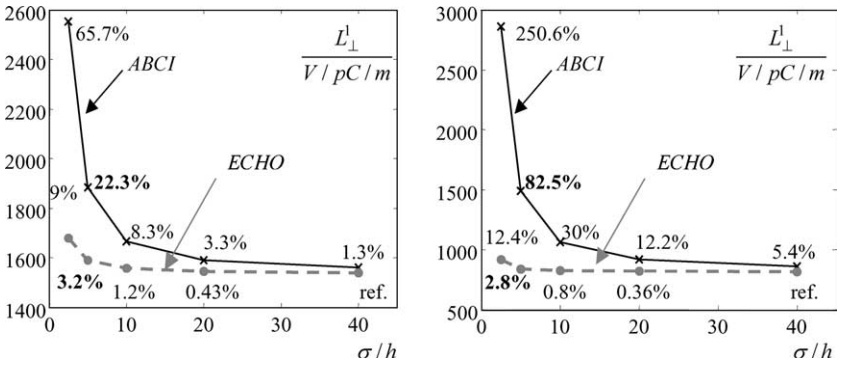

Fig. 8. The transverse dipole loss factor $L_\perp^1$ for the collimators with $L = 10$ cm (left) and $L = 20$ cm (right). The solid lines show the results from the code ABCI and the dashed lines display the results from the ECHO code. The relative errors are given regarding the reference value (marked as ref. on the graphs) calculated by ECHO with the finest mesh.

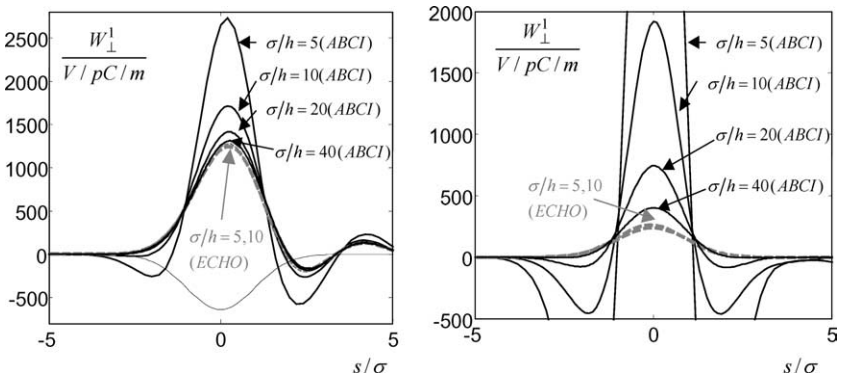

Fig. 9. The transversal dipole wake function for the collimators with $L = 20$ cm (left) and $L = 100$ cm (right). The solid curves show the results from the code ABCI and the dashed lines represent the results from the code ECHO. The low curve (left) outlines the charge distribution in the Gaussian bunch.

results for the ECHO and the solid ones for ABCI 9.2.1 [20]. In Fig. 8(right) the transversal dipole loss factor $L_\perp^1$ for the collimator with $L = 20$ cm is shown.

Fig. 9 shows the transversal dipole wake potential $W_\perp^1(s)$ for collimators with $L = 20$ cm and $L = 100$ cm. The solid curves show results for ABCI and the dashed ones show results for the new scheme.

From the above examples we see that the absolute error for the new code ECHO remains approximately on the same level independently from the length of the collimator. The reference code ABCI demands a much more dense mesh for the same accuracy, strongly depending on the collimator length. In the last example even with 40 points on σ the error for ABCI is in excess of 100%.

Finally, we show in Fig. 10 the dipole wake potentials of a Gaussian bunch with $\sigma = 1$ mm for the TESLA cryomodule of total length ~11 m [21] containing eight nine cell cavities and nine bellows as shown in Fig. 11. The moving mesh in the last example covers the bunch longitudinally in the range from -5σ to 100σ. The length of the moving mesh is only 0.105 m which allows to reduce drastically the computational demands (storage and CPU time) compared to the stationary mesh of total length ~11 m.

As our experience shows, the scheme allows to calculate the wake fields of ultra-short bunches ($\sigma \sim 25$ μm) in accelerator structures of several tens meter length on a standard PC.

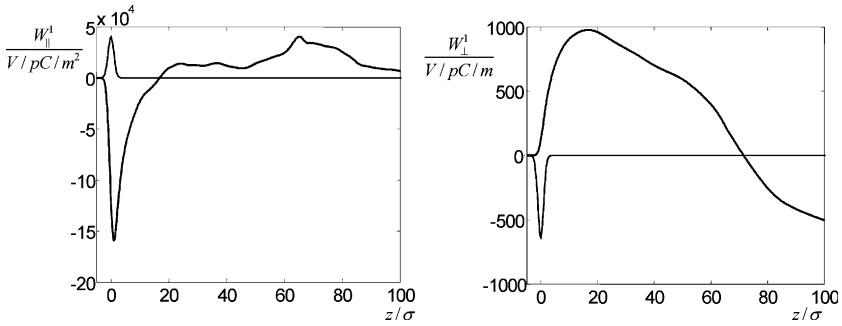

Fig. 10. The dipole wakes for the TESLA cryomodule and Gaussian bunch with RMS length $\sigma = 1$ mm.

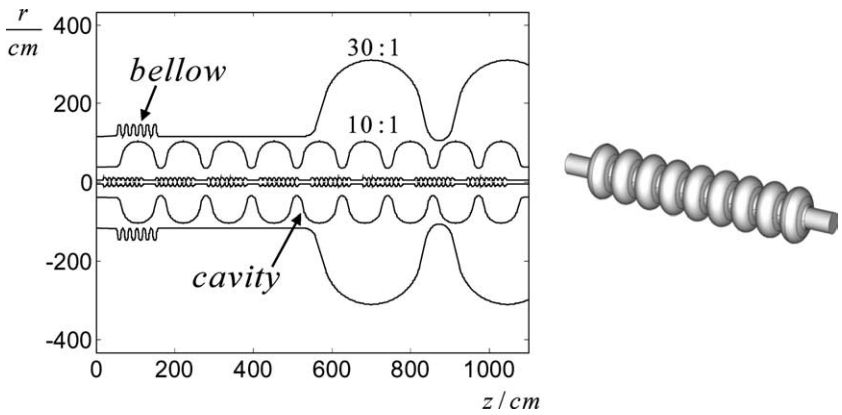

Fig. 11. The geometry of the TESLA cryomodule (left) and the TESLA cavity (right).

9. Conclusions

A new implicit scheme for the calculation of electromagnetic fields in the vicinity of relativistic electron bunches was introduced. As shown by several numerical examples the scheme is able to model curved boundaries with high accuracy and allows for a non-deteriorating calculation of the field solution for very long times. The high overall accuracy of the scheme was demonstrated for realistic collimator problems. The scheme allows to use a moving mesh and thus to calculate wake fields of very short bunches for a range of problems, where presently available codes experience severe problems.

Acknowledgements

The authors thank A.Novokhatski and K.Bane for encouragement of the work.

References

[1] W.C. Chao, Physics of Collective Beam Instabilities in High Energy Accelerators, Wiley, New York, 1993.
[2] T. Weiland, On the numerical solution of Maxwell's equations and applications in accelerator physics, Particle Accelerators 15 (1984) 245.

[3] V. Balakin, A. Novokhatski, VLEPP: longitudinal beam dynamics, in: Proc. of the 12-th Int. Conference on High-Energy Accelerators, Fermilab, 1983.
[4] O. Meincke, A.Wagner, B. Zotter, New wake field and bunch lengthening codes, SL-Note-97-17(AP), CERN, 1997.
[5] I. Zagorodnov, R. Schuhmann, T. Weiland, A uniformly stable conformal FDTD-method on cartesian grids, Int. J. Numer. Model. 16 (2003) 127.
[6] T. Weiland, A discretization method for the solution of Maxwell's equations for six-component fields, Electron. Commun. (AEÜ) 31 (1977) 116.
[7] T. Weiland, Time domain electromagnetic field computation with finite difference methods, Int. J. Numer. Model. 9 (1996) 295.
[8] T. Weiland, On the unique numerical solution of Maxwellian eigenvalue problems in three dimensions, Particle Accelerators 17 (1985) 227.
[9] K. Bane, T. Weiland, Wake force computation in the time domain for long structures, in: Proc. of the 12th International Conference on High Energy Accelerators, vol. 314, Chicago, 1983.
[10] A. Taflove, S.C. Hagness, Computational Electrodynamics: The Finite-Difference Time-Domain Method, Artech House, London, 2000.
[11] T. Weiland, On the computation of resonant modes in cylindrically symmetric cavities, Nucl. Instr. Meth. 216 (1983) 329.
[12] A. Novokhatski, M. Timm, T. Weiland, Transition dynamics of the wake fields of ultra short bunches, in: Proc. of the ICAP 1998, vol. 132, Monterey, California, USA, 1998.
[13] T. Weiland, Transverse beam cavity interaction, Part I: short range forces, Nucl. Instr. Meth. 212 (1983) 13.
[14] S. Dey, R. Mittra, A locally conformal finite-difference time-domain (FDTD) algorithm for modeling three-dimensional perfectly conducting objects, IEEE Microwave Guided Wave Lett. 7 (9) (1997) 273.
[15] B.W. Zotter, S.A. Kheifets, Impedances and Wakes in High-Energy Particle Accelerators, World Scientific, London, 1998.
[16] T. Weiland, Comment on wake field computation in time domain, Nucl. Instr. Meth. 216 (1983) 31.
[17] O. Napoly, Y. Chin, B. Zotter, A generalized method for calculating wake potentials, Nucl. Instr. Meth. 344 (1993) 255.
[18] W.K.H. Panofsky, W.A. Wenzel, Some considerations concerning the transverse deflection of charged particles in radio-frequency fields, Rev. Sci. Instr. 27 (1956) 947.
[19] K. Yokoya, Impedance of slowly tapered structures, Tech. Rep. SL/90-88 (AP), CERN, 1990.
[20] Y.H. Chin, User's guide for ABCI Version 8.7, CERN-SL-94-02-AP, CERN, 1994.
[21] TESLA Technical Design Report, DESY 2001-011, Hamburg, Germany, 2001, Part II.